Journal of Structural Biology 183 (2013) 441–454

Contents lists available at SciVerse ScienceDirect

Journal of Structural Biology

journal homepage: www.elsevier.com/locate/yjsbi

Biomineralization in living hypercalcified demosponges: Toward a shared mechanism?

Melany Gilis [a,b,*], Olivier Grauby [c], Philippe Willenz [a,b], Philippe Dubois [b], Vasile Heresanu [c], Alain Baronnet [c]

[a] Department of Invertebrates, Royal Belgian Institute of Natural Sciences, B-1000 Brussels, Belgium
[b] Laboratoire de Biologie marine, Université Libre de Bruxelles, B-1050 Brussels, Belgium
[c] Aix-Marseille Université and Centre Interdisciplinaire de Nanosciences de Marseille (CINaM), Campus de Luminy, F-13288 Marseille, France

ARTICLE INFO

Article history:
Received 22 February 2013
Received in revised form 24 May 2013
Accepted 29 May 2013
Available online 6 June 2013

Keywords:
Hypercalcified sponges
Biomineral
Calcification
Porifera
Calcium carbonate
Demospongiae

ABSTRACT

Massive skeletons of living hypercalcified sponges, representative organisms of basal Metazoa, are uncommon models to improve our knowledge on biomineralization mechanisms and their possible evolution through time. Eight living species belonging to various orders of Demospongiae were selected for a comparative mineralogical characterization of their aragonitic or calcitic massive basal skeleton. The latter was prepared for scanning and transmission electron microscopy (SEM and TEM), selected-area electron diffraction (SAED) and X-ray diffraction (XRD) analyses. SEM results indicated distinctive macro- and micro-structural organizations of the skeleton for each species, likely resulting from a genetically dictated variation in the control exerted on their formation. However, most skeletons investigated shared submicron to nano-scale morphological and crystallographical patterns: (1) single-crystal fibers and bundles were composed of 20 to 100 nm large submicronic grains, the smallest structural units, (2) nano-scale likely organic material occurred both within and between these structural units, (3) {1 1 0} micro-twin planes were observed along aragonitic fibers, and (4) individual fibers or small bundles protruded from the external growing surface of skeletons. This comparative mineralogical study of phylogenetically distant species brings further evidence to recent biomineralization models already proposed for sponges, corals, mollusks, brachiopods and echinoderms and to the hypothesis of the universal and ancestral character of such mechanisms in Metazoa.

1. Introduction

Among more than 8500 valid Recent sponge species known today (van Soest et al., 2012), only a few ones produce a massive basal skeleton of calcium carbonate, in addition to a siliceous or calcareous spicule framework. These so-called hypercalcified sponges, luxuriant reef-builders of late Paleozoic and Mesozoic eras, were considered to be extinct until a handful of living species were rediscovered almost half a century ago. Scuba diving and submersible explorations allowed to extend our knowledge on these coralline sponges with the discovery of nearly twenty new living species found almost exclusively in cryptic or deep habitats in tropical seas and the Mediterranean (Hartman, 1969, 1979; Hartman and Goreau, 1970, 1975, 1976; Vacelet, 1964, 1970; Vacelet and Lévi, 1958; Willenz and Pomponi, 1996). Recent hypercalcified sponges form a polyphyletic group with species belonging to various orders of both Calcarea and Demospongiae. The occurrence of a massive calcareous basal skeleton in these living forms was considered as an archaic character that would have appeared in most Paleozoic and Mesozoic taxa (Reitner, 1992; Vacelet, 1979, 1985). As some of their skeletal features are often analogous to their fossil relatives, Ca-carbonate biomineralization of these sponges was considered to be a conservative process maintained since million of years (Gautret et al., 1996; Lange et al., 2001; Reitner, 1992; Reitner and Engeser, 1987; Reitner et al., 1997, 2001; Vacelet, 1983; Wörheide, 1998). Although these evolutionary assumptions would need further demonstration, these unique Recent sponges represent valuable models to improve our understanding of the early evolution of Ca-carbonate biomineralization mechanisms.

Nonetheless, among skeletons of even phylogenetically closely related living hypercalcified species, highly diverse macro- and microstructures, organization grades, elemental/isotopic chemistry and associated organic macromolecules were described (see for review Reitner, 1992; Vacelet et al., 2010) leading authors to suggest different mineralization mechanisms. For instance, while most

* Corresponding author. Present address: Laboratory for Biological Geochemistry, Ecole Polytechnique Fédérale de Lausanne, ENAC IIE LGB, GR C1 507, Station 2, Switzerland.
E-mail address: melany.gilis@epfl.ch (M. Gilis).

1047-8477/$ - see front matter © 2013 Elsevier Inc. All rights reserved.
http://dx.doi.org/10.1016/j.jsb.2013.05.018

previous investigations highlighted an extracellular biomineralization of basal skeleton in living hypercalcified sponges (Reitner and Gautret, 1996; Reitner et al., 2001; Willenz and Hartman, 1989; Gilis et al., 2012), the demosponge *Astrosclera willeyana* initiates the formation of its spherulitic basal skeleton through an intracellular pathway followed by a secondary extracellular growth phase (Lister, 1900; Wörheide, 1998; Wörheide et al., 1997). Wörheide (1998) provided a detailed description of biomineralization processes in this species combining three mechanisms: (1) small skeletal spherulites are formed within large vacuole cells (LVC) in the ectosome; (2) 15–20 μm large spherulites are further carried by a group of another cell type into the extracellular space, between the soft tissue and the growing skeleton, where they fuse together through secondary epitaxial growth; (3) a withdrawal of the soft tissue produces spaces in the lowermost-part of the skeleton cavities which are then filled by the epitaxial growth of spherulitic fibers. More recently, Jackson et al. (2010) have shown that intracellularly degraded bacteria were used as an organic matrix for controlling the formation of spherulites in the LVC like cells of *A. willeyana*. Furthermore, these authors discovered that the gene encoding for a matrix protein occurring in the calcified spherulite would be horizontally acquired by this sponge from a bacterium (Jackson et al., 2011). In *Acanthochaetetes wellsi*, the only known living hypercalcified demosponge producing a Mg-calcite basal skeleton, the extracellular mineralization of calcitic fibers would take place in four different locations of the skeleton, each involving a different biomineralization mechanism (Reitner and Gautret, 1996).

Although these previous macro- and microstructural mineralogical studies suggest a divergent evolution of biomineralization modes among living hypercalcified sponges, some recent observations at higher magnifications might contrarily indicate some shared pathways of biomineralization at lower scales. For example, 50–100 nm large grains that have been universally described as the smallest structural units in most calcium carbonate skeletons produced by metazoans (e.g. Cuif and Dauphin, 2005a,b; Cuif et al., 2008, 2011; Cusack et al., 2008; Goetz et al., 2011; Isa, 1986; Jacob et al., 2008; Pérez-Huerta et al., 2013; Robach et al., 2005; Rousseau et al., 2005; Schmahl et al., 2012a,b; Sethmann et al., 2006; Sethmann and Wörheide, 2008; Stolarski, 2003; Stolarski and Mazur, 2005; Weiner and Addadi, 2011) also occur in the three Recent hypercalcified demosponges species *Vaceletia crypta*, *A. willeyana* and *Ceratoporella nicholsoni* (Cuif et al., 2011) as well as in the skeleton of the living Mediterranean hypercalcified sponge *Petrobiona massiliana*, belonging to Calcarea (Gilis et al., 2011; Stolarski and Mazur, 2005).

These skeletal submicronic structures were shown to be in a transient amorphous state before crystallization during the formation of calcium carbonate skeleton in mollusk (Baronnet et al., 2008; Cuif et al., 2008, 2011; Jacob et al., 2008; Wehrmeister et al., 2011; Weiss et al., 2002), brachiopods (Goetz et al., 2011; Griesshaber et al., 2009; Schmahl et al., 2012a) and echinoderms (Beniash et al., 1997; Gong et al., 2012; Killian et al., 2009; Ma et al., 2007; Politi et al., 2004, 2006, 2008; Raz et al., 2003). Crystallization would progressively propagate through those pre-assembled submicronic amorphous grains, producing micron-scale monocrystal-like structures (Baronnet et al., 2008; Cuif et al., 2008; Cusack et al., 2008; Goetz et al., 2011; Jacob et al., 2008; Killian et al., 2009; Nouet et al., 2012; Politi et al., 2008; Przeniosło et al., 2008; Schmahl et al., 2012a,b; Weiner and Addadi, 2011), a biomineralization model also suggested for calcareous sponge spicule production (Sethmann et al., 2006; Sethmann and Wörheide, 2008) and basal skeleton formation in the hypercalcified sponge *P. massiliana* (Gilis et al., 2011).

In order to validate whether this pattern of biomineralization also prevails in phylogenetically distinct hypercalcified sponges, we investigated the basal skeleton of eight recent demosponges species, from macro- to submicronic structures, by scanning and transmission electron microscopy (SEM and TEM), electron microdiffraction (SAED) and X-ray diffraction analyses (XRD).

2. Materials and methods

Specimens of eight different living hypercalcified sponge species were collected by scuba diving and submersible explorations (Table 1). Samples were immediately preserved in ethanol 70° after collection. Before analyses, samples of each species were treated identically. Fragments were shortly exposed to a 10% sodium hypochlorite solution in order to remove superficial soft tissues. Skeletons were dehydrated in a graded ethanol series and stored in absolute ethanol until further treatments for scanning and transmission electron microscopy (SEM and TEM) and X-ray diffraction (XRD) analyses.

For SEM, samples were fractured, dried at 50 °C, mounted on aluminum stubs, carbon-coated and observed on a SEM JEOL JSM-6320F at 15 kV.

For TEM, small fragments were gently-crushed in a mortar and pestle. Resulting micron- or submicron-scale particles were mounted on holey carbon coated copper grids. Air-dried preparations were then observed on a JEOL 3010 TEM at 300 kV for TEM imaging and recording selected area electron diffraction (SAED) patterns. A low dose illumination during tuning of the objective focus and astigmatism correction was carefully used to reduce damages to biogenic carbonate. SAED diagrams were obtained by using a set of apertures, selecting skeleton areas with homogenous absorption/diffraction contrasts. A simple-tilt specimen holder was used since we intended to check only the crystallinity of the microstructures, not their local crystallography.

For XRD, finer powders were obtained for each species in a mortar and pestle. Powder diffraction measurements were realized using an INEL diffractometer fitted with a 120° curved position sensitive detector (CPS-120), working in transmission mode, and equipped with a Cu anticathode (λ = 1.5418 Å) operated at 45 kV and 20 mA. Each sample powder was X-rayed separately in thin-walled (0.5 and 0.7 mm) capillary tubes for X-ray diffraction. For better accuracy, pure α-quartz was used as internal standard.

The basal skeleton of each species was investigated from macrostructure to submicronic structure. In order to identify skeleton growth steps, observations were systematically focused on micronic and submicronic structural units in internal mature areas of the skeleton exposed by fracturing, as well as in growing superficial layers. Selected area electron diffraction (SAED) patterns on TEM images and X-ray diffraction analysis on gently-crushed powders allowed to characterize respectively the amorphous, single- or poly-crystalline nature of the selected material in micronic to submicronic structures and to specify the crystalline phase(s) present in each basal skeleton.

3. Results

All morphological (SEM and TEM) and crystallographical (SAED and XRD) observations are presented individually for each species and summarized in Table 2.

3.1. Acanthochaetetes wellsi

The basal skeleton of *A. wellsi* was made up of contiguous vertical tubes (calicles) 300–400 μm wide, subdivided by horizontal tabulae delineating inter-tabular spaces (Fig. 1a). Short spines sparsely ornamented walls of calicles, 50–100 μm large. The lamellar microstructure of walls, spines and tabulae were composed of

Table 1
Taxonomic arrangement and collection data of the eight hypercalcified demosponges species investigated.

Species	Location & Depth	Collectors
Order HADROMERIDA	**Watom Island, New Guinea (−20 m)**	Kelly
Acanthochaetetes wellsi Hartman & Goreau 1975	(Lat 4°6′52.34″S, Long 152°5′27.69″E)	16/10/1991
Willardia caicosensis Willenz & Pomponi 1996	**Grand Turk Island, Bahamas (−111 m)**	Willenz et al.
	(Lat 21°31′62″N, Long 71°08′04″W)	24/11/1994
Order AGELASIDA	**Watom Island, New Guinea (−20 m)**	Kelly
Astrosclera willeyana Lister 1900	(Lat 4°6′52.34″S, Long 152°5′27.69″E)	16/10/1991
Ceratoporella nicholsoni Hickson 1911	**Pear Tree Bottom, North Jamaica (−28 m)**	Willenz
	(Lat 18°27′57.31″N, Long 77°21′18.49″W)	03/05/1987
Goreauiella auriculata Hartman 1969	**Pear Tree Bottom, North Jamaica (−28 m)**	Willenz
	(Lat 18°27′57.31″N, Long 77°21′18.49″W)	01/05/1987
Hispidopetra miniana Hartman 1969	**Turk & Caicos Islands, Bahamas (−133 m)**	Willenz et al.
	Lat 21°00.608′N, Long 70°51.113′W)	20/11/1994
Stromatospongia norae Hartman 1969	**Pear Tree Bottom, North Jamaica (−28 m)**	Willenz
	(Lat 18°27′57.31″N, Long 77°21′18.49″W)	01/05/1987
Order HAPLOSCLERIDA	**Acklins Island, Bahamas (−30 m)**	Willenz
Calcifibrospongia actinostromarioides Hartman 1979	(Lat 22°9′33.03″N, Long 74°18′54.46″W)	07/08/1985

elongated fibers and bundles oriented parallel to the surface of those skeletal structures and tangentially around wall perforations, the latter likely corresponding to soft tissue anchorage spots (Fig. 1b). Fibers, 75–200 nm in diameter reaching up to several micrometers in length, always presented a more electron-emitting elongated core in SEM (Fig. 1c). While this central core was proved to be crystalline by TEM (Fig. 1d, d'), its precise nature still needs to be clarified. Furthermore, in recently deposited fibers covering internal surface of walls, organic and/or mineral bridges seemed to link individual adjacent fibers (Fig. 1c). SAED patterns demonstrated that fibers were single crystals of calcite each (Fig. 1d'), adjacent ones forming monocrystalline bundles to some extent (Fig. 1e–g). For example, the single-crystal element presented on Fig. 1f (bright field) and Fig. 1g (dark field) was a bundle of two fibers with a thin material, likely organic, at their contact boundary that seemed to generate slight misorientations of the crystal lattice according to the thin moiré patterns at their junction where they overlap (Fig. 1f–g). In addition, within all longitudinally sectioned fibers and bundles, dark field imaging allowed enhancing transverse striations 10–15 nm apart (Fig. 1g). In all fibers and bundles, we observed a submicronic structure composed of granular units 50–100 nm in size in SEM (Fig. 1e). Smaller submicronic grains were also observed in TEM when clustered into a polycrystalline structure (Fig. 1i, i') probably filling spaces between tangentially oriented fibers and bundles (Fig. 1h). Finally, randomly entangled single crystalline Mg-calcite bundles with sharper polygonal faces filled inter-tabular spaces (Fig. 1j, k).

3.2. Willardia caicosensis

Delicate finger-like pillars, 1–2 mm high and 200–700 μm wide, covered the relatively thin basal portion of the aragonitic skeleton of *W. caicosensis* (Fig. 2a). The skeleton was made of fascicular microstructures (Fig. 2b). In fracture of mature skeleton layers, fiber and bundle units were barely perceptible due to their peculiar highly granular aspect (Fig. 2b, c). Submicronic grains 50–100 nm wide in SEM (Fig. 2c) composed the basal skeleton of *W. caiconsensis* and were assembled into single-crystal fibers, 70–150 nm in diameter (Fig. 2d, d'). Along these fibers, we noticed lighter transverse striations 2–5 nm apart (Fig. 2d), which became even more pronounced after short exposition under the electron beam. Adjacent fibers, often slightly radiating, were themselves associated into monocrystalline bundles (Fig. 2e, e') while randomly packed submicronic grains formed polycrystalline clusters (Fig. 2d, d''). At the surface of the skeleton, growing layers displayed emerging individual granular fibers or small bundles (Fig. 2f).

3.3. Astrosclera willeyana

The first intracellularly formed aragonitic spherulites were isolated from the skeleton by dissolution of the soft tissue of *A. willeyana* with sodium hypochlorite (Fig. 3a). Intracellular spherulites, 10–20 μm in diameter, were composed of radiating granular fibers, 50–120 nm in width, mostly fused in small bundles (Fig. 3b).

Table 2
Comparative table of mineralogical observations made on the basal skeleton of hypercalcified sponges species belonging to Calcarea (from Gilis et al. 2011) and Demospongiae (present study). Ca-carbonate polymorphs were determined by powder X-ray diffraction analysis. The size of submicronic grains is estimated only from SEM observations.

	Polymorph	Microstructure	Fibre diameter	Submicronic grain diameter (in SEM)	Higher single-crystal structural unit	Transverse striations	Micro-twin planes	Growing individual fibres
CALCAREA								
P. massiliana (Gilis et al. 2011)	Mg-calcite	Fibroradiated along an axis	50–100 nm	50-100 nm	Fibre Bundle	Not observed	Not observed	Yes
DEMOSPONGIAE								
A. wellsi	Mg-calcite	Mg-calcite	75–200 nm	50–100 nm	Fibre Bundle	Yes	Not observed	Not observed
W. caicosensis	Aragonite	Aragonite	70–150 nm	50–100 nm	Fibre Bundle	Yes	Yes	Yes
A. willeyana	Aragonite	Aragonite	50–120 nm	50–100 nm	Fibre Bundle	Yes	Yes	Yes
C. nicholsoni	Aragonite	Aragonite	50–120 nm	50–100 nm	Fibre Bundle	Yes	Yes	Yes
G. auriculata	Aragonite	Aragonite	60–100 nm	50–100 nm	Fibre Bundle	Yes	Yes	Yes
H. miniana	Aragonite	Aragonite	75–150 nm	75–100 nm	Fibre Bundle	Yes	Yes	Yes
S. norae	Aragonite	Aragonite	50–150 nm	50–100 nm	Fibre Bundle	Yes	Yes	Yes
C. actinostromarioides	Aragonite	Aragonite	50–150 nm	50–100 nm	Fibre Bundle	Yes	Not observed	Less obvious

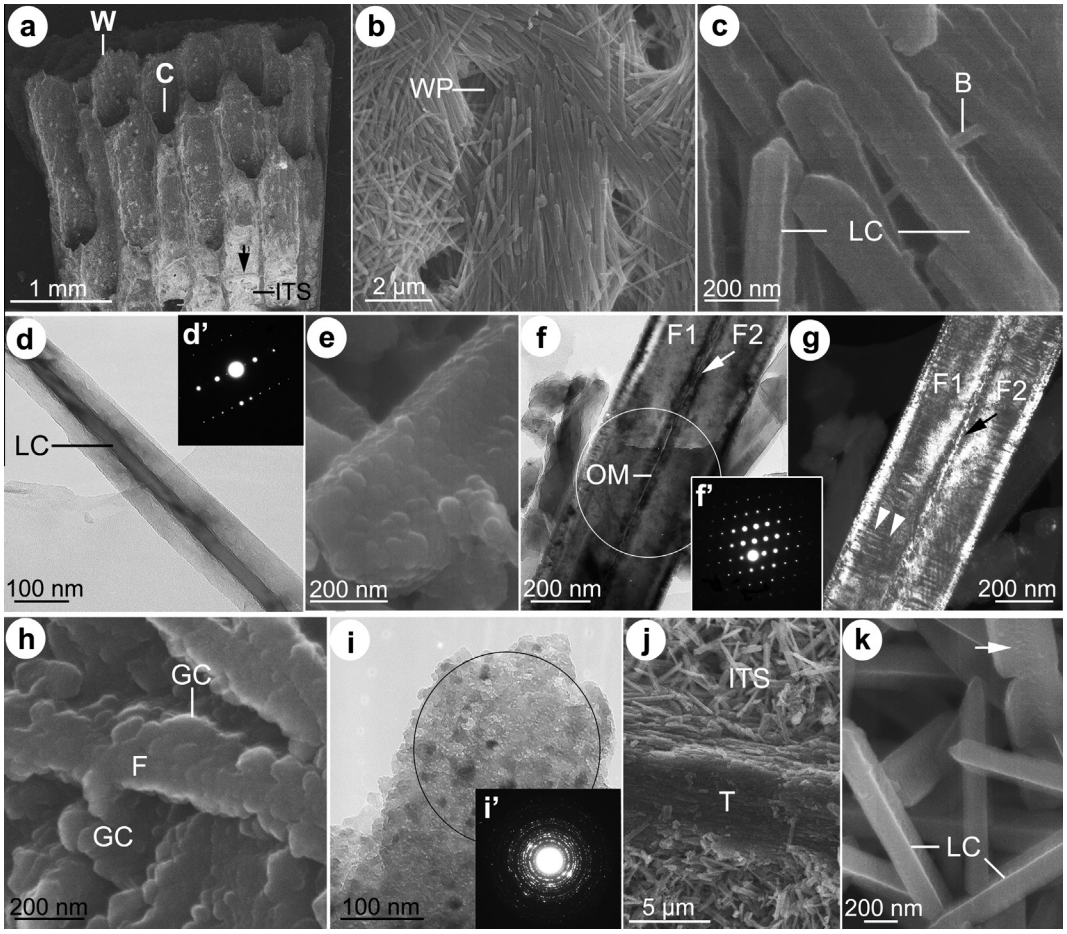

Fig.1. Mg-calcite basal skeleton of *Acanthochaetetes wellsi*. (a) Macrostructural organization with vertical calicles subdivided by horizontal tabulae (black arrow) (SEM). (b) Lamellar microstructure in wall of a calicle with elongated fibers tangentially organized around wall perforations (SEM). (c) Mg-calcite individual granular fibers in early growth zone with internal longitudinal more electron-emitting core and tiny bridges between fibers (SEM). (d, d') TEM side view of individual fiber in longitudinal section with single-crystal behavior (SAED selection: whole fiber width) and a longitudinal strongly crystalline core. (e) View of a small bundle of fibers made of 50–100 nm wide granular units (SEM). (f) TEM bright field image of two parallel fibers in a bundle with a thin organic material squeezed between them producing moiré patterns (white and black arrows for respectively f and g). (f') Monocrystalline electron diffraction pattern from the encircled area of (f). (g) TEM dark field view of the area as in (f) enhancing thick transverse striations in both fibers of the bundle (white arrowheads). (h) Clusters of submicronic grains filling spaces between tangential fibers (SEM). (i, i') Polycrystalline cluster of submicronic grains in TEM (black circle: SAED selection). (j) SEM view of horizontal tabula in a calicle formed by similar granular bundles of fibers. (k) Randomly arranged single-crystal Mg-calcite bundles showing sharper polygonal faces (SEM). C: calicle, B: bridge, F: fiber, GC: granular cluster, ITS: inter-tabular space, LC: longitudinal core, OM: organic matrix, T: tabula, W: wall, WP: wall perforation.

At the surface of the basal skeleton, spherulites displayed signs of a secondary growth event. Fibers were elongated, interweaving from one spherulite to another, binding them to each other (Fig. 3c) to form the massive skeleton organized as a fine reticulum (Fig. 3d). As intracellularly formed spherulites sized at maximum 20 µm in diameter, the spherical-shaped intracellular growth zone (i.e. <10 µm radius from the centre of spherulites) could be theoretically discerned from its extracellular growth zone (i.e. >10 µm radius of spherulites); this was even more obvious when the mature spherulites reached an ovoid shape (Fig. 3e). Interestingly, the same granular submicronic structures were observed in SEM in both zones: radiating fibers assembled in larger bundles were made up of 50–100 nm granular structural units (Fig. 3f, g). In addition, the centre of spherulites was composed of a large cluster of these submicronic grains. In TEM, while the granular morphology of fibers/bundles was still obvious thanks to the organic electron-translucent material surrounding submicronic structural units, the latter appeared to be under 50 nm in diameter (Fig. 3h). Furthermore, after a short time under the electron beam, transverse striations, with a slightly larger period (5–15 nm), also appeared in bundles, revealing the occurrence of a rapidly altering material (Fig. 3i). Bundles of fibers showed micro-twin or stacking-fault planes aligned along the fiber axis (Fig. 3j). Nevertheless SAED analysis revealed that bundles, and therefore fibers, were single-crystal structural units (Fig. 3k, k'). The external surface of spherulites undergoing extracellular growth displayed emerging individual granular fibers or small bundles (Fig. 3l, m).

3.4. Ceratoporella nicholsoni

The aragonitic basal skeleton of *C. nicholsoni* was made up of a massive basal portion with apical contiguous vertical calicles extending down to 1 mm into the skeleton (Fig. 4a). The microstructure of walls delineating calicles as well as the bottom of the latter (“infilling zone”) was a fascicular arrangement of crystalline bundles (Fig. 4b) composed of submicronic granular structures (Fig. 4c). Fibers, around 100 nm in diameter, were laterally assembled into single crystal bundles (Fig. 4d, d'). Transverse striations, 2–5 nm apart, occurred rapidly under the electron beam, evident under direct observation although less visible in the picture (Fig. 4d), as well as micro-twin or stacking-fault planes (not shown). Emerging granular individual fibers and bundles were seen in growing superficial areas of the skeleton, i.e. at the top of walls (Fig. 4e, f) and at the bottom of calicles (Fig. 4g, h). Additional

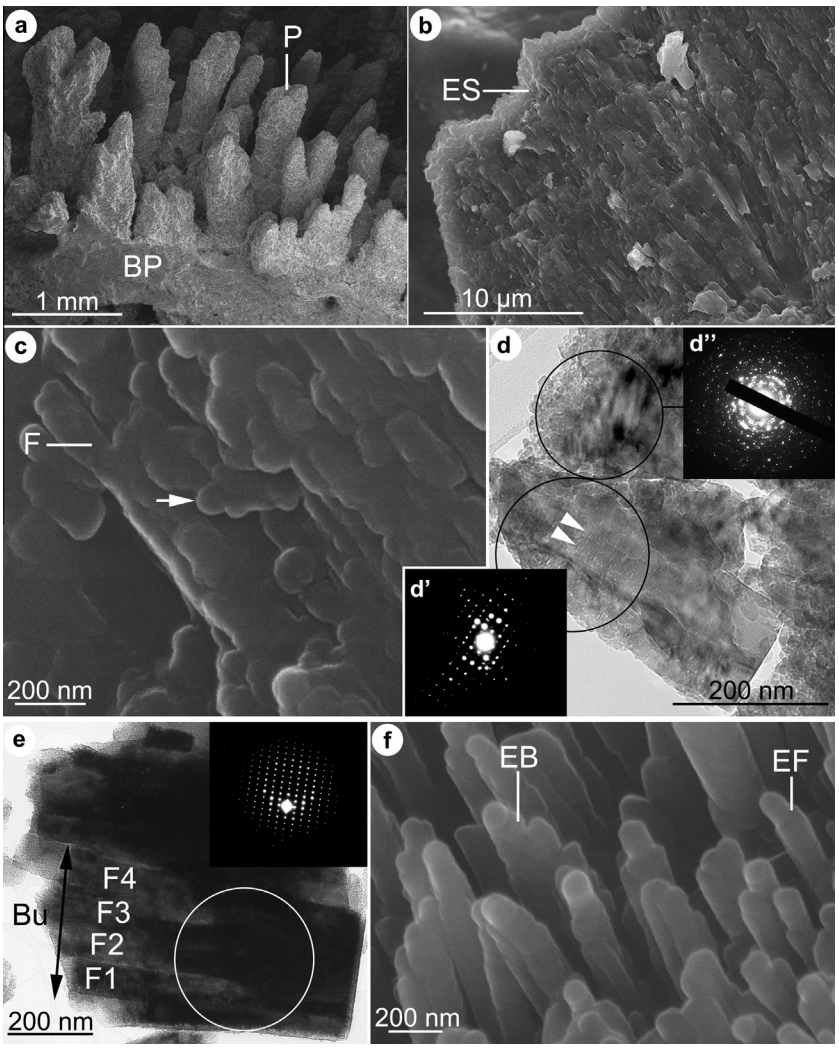

Fig.2. Aragonitic basal skeleton of *Willardia caicosensis*. (a) Macrostructure with delicate finger-like pillars covering the thin basal portion (SEM). (b) Fascicular microstructural organization of highly granular bundles of fibers (SEM). (c) Bundles at higher magnification in SEM with strongly marked granular relief (white arrow). (d) TEM detail of a single crystal fiber (d') with transverse thin striations (white arrowheads) and a polycrystalline cluster (d'') (lower and upper black circles: SAED selection of respectively d' and d''). (e, e') TEM and SAED view of a monocrystalline bundle comprising more than four slightly radiating adjacent fibers (white circle: SAED selection). (f) Superficial growing layer of the skeleton with emerging individual granular fibers or bundles (SEM). BP: basal part, Bu: bundle, EB: emerging bundle, EF: emerging fiber, ES: external skeletal surface, F: fiber, P, pillar.

clusters of closely packed submicronic grains often appeared between fibers and bundles in SEM (Fig. 4f, h). These clusters seemed to contain 30–50 nm granular units like in fibers (Fig. 4i), although SAED analysis demonstrated their polycrystalline behavior (Fig. 4i').

3.5. Goreauiella auriculata

Arborescent processes arising from a reticulate macrostructure distinguished the aragonitic basal skeleton of *G. auriculata* (Fig. 5a). Crystalline bundles of fibers, organized in a fascicular microstructure (Fig. 5b), presented a submicronic granular morphology (Fig. 5c). The surface of the basal skeleton showed typically incurved individual growing fibers with diameter ranging from 60–100 nm presenting a globular tip (Fig. 5d). In TEM, these incurved fibers were easily recognized (Fig. 5e) and their monocrystalline diffraction pattern (Fig. 5e') as well as their coherent assemblage into larger single crystal bundles (Fig. 5f, f') were demonstrated by SAED. Transverse fractures of crystalline fibers and bundles produced clear plane surfaces in SEM (Fig. 5g) and TEM (Fig. 5h, i). Furthermore, in SEM, the fracture of some bundles showed a hexagonal outline (Fig. 5g). Finally, TEM features demonstrated the occurrence of lighter striations, 5–15 nm apart during imaging (Fig. 5h), and longitudinal micro-twin/stacking-fault planes (Fig. 5i) as well as organic thin material at fibers and bundles boundaries.

3.6. Hispidopetra miniana

The aragonitic basal skeleton of *H. miniana* bore numerous arborescent and knoblike processes up to 5 mm high, ornamented by smaller spine-like elements a few hundred micrometers high (Fig. 6a, b). The latter presented bumps or rounded spines up to 25 µm high at their surface (Fig. 6b). Bundles of crystalline fibers radiated in a fascicular organization (Fig. 6b). Granular structural units, 20–100 nm wide, formed the fibrillar submicronic structure of the aragonitic skeleton in SEM (Fig. 6c, f and i) and TEM (Fig. 6d). Single crystal fibers, 75–150 nm in diameter (Fig. 6e, e') formed larger monocrystalline bundles (Fig. 6f, g and g'). However, a central interruption of Bragg contrasts crossing these bundles suggested the presence of an amorphous core. Lighter transverse striations, 3–10 nm apart, appeared rapidly under the electron-beam in TEM (Fig. 6h) as well as longitudinal translucent material at fiber boundaries (Fig. 6h). In addition, fibers also showed some

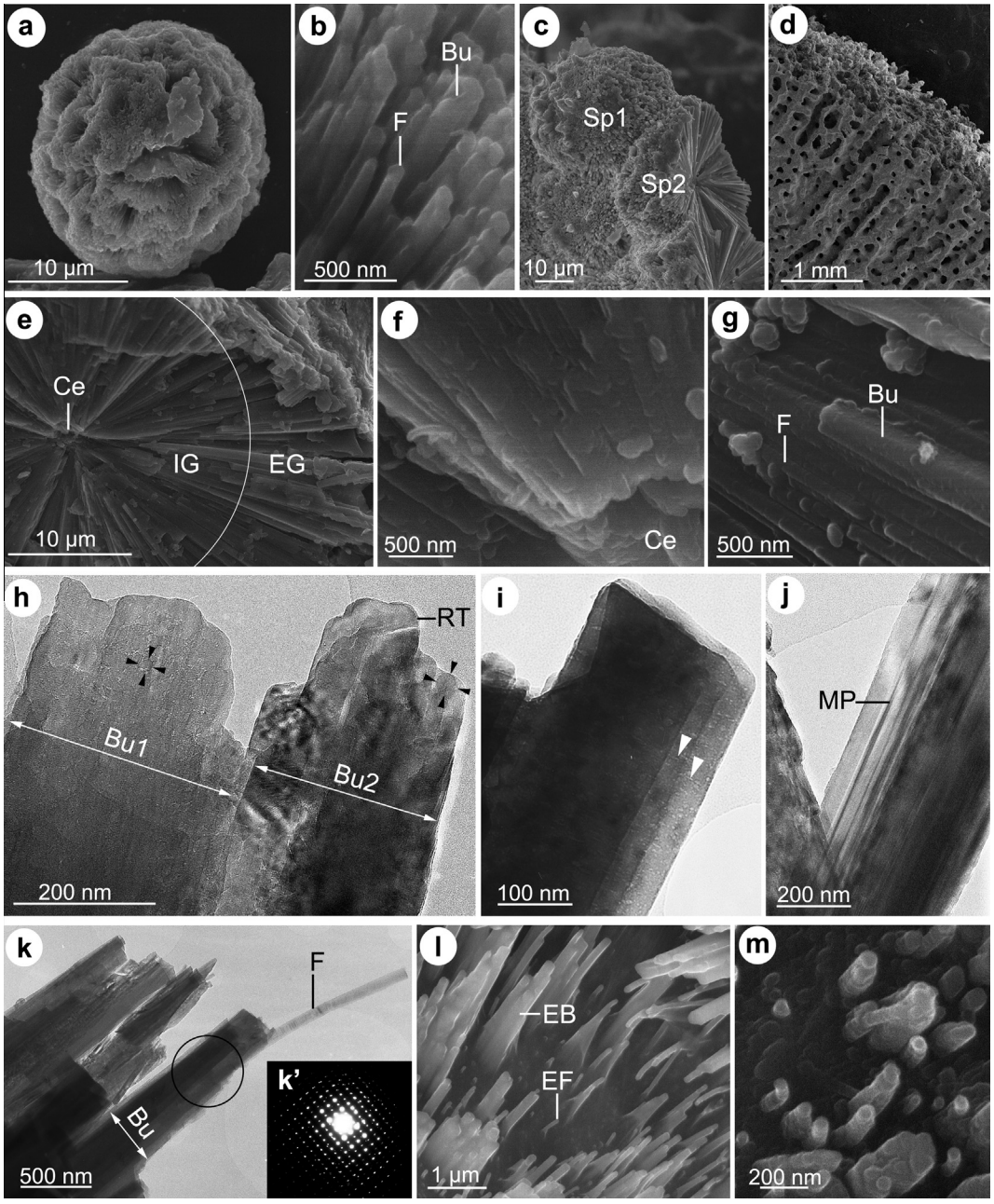

Fig.3. Aragonitic basal skeleton of *Astrosclera willeyana*. (a) Intracellularly formed spherulite isolated from the soft tissue (SEM). (b) Radiating granular fibers 50–100 nm large and bundles of the intracellularly formed spherulite (SEM). (c) Intracellularly formed spherulites released from the soft tissue growing at the surface of the basal skeleton during the secondary extracellular growth (SEM). (d) Reticulate macrostructural organization of the basal skeleton with branches composed of aragonitic spherulitic structural elements (SEM). (e) Fractured egg-shaped spherulite in the skeleton (SEM). The white line delineates approximately and theoretically intracellular (IG) and extracellular (EG) growth zones. (f) Higher magnification of the intracellularly formed radiating fibers and bundles near the center of the spherulite, showing their submicronic granular structure (SEM). (g) Higher magnification of the extracellularly formed radiating fibers and bundles showing similar submicronic granular structures (SEM). (h) Two adjacent bundles with rounded tips build up by the internal granular submicronic structures (delineated by black arrowheads) of their fibers (TEM). (i) Fractured bundle with internal transverse thin striations (white arrowheads) (TEM). (j) Micro-twin planes oriented along the bundle axis (TEM). (k) Superficial bundles with an emerging individual fiber (TEM). SAED pattern (k') indicating the single-crystal behavior of the selected bundle (black circle). (l) Emerging individual granular fibers or small bundles on the external surface of spherulites undergoing extracellular growth (SEM). (m) Higher magnification of emerging fibers and bundles illustrating their granular structure (SEM). Bu: bundle, Ce: center, EB: emerging bundle, EF: emerging fiber, EG: extracellular growth zone, F: fiber, IG: intracellular growth zone, MP: micro-twin plane, Sp: spherulite.

longitudinal micro-twin/stacking-fault planes. Finally, highly granular growing fibers and bundles protruded from the apical surface of the skeleton (Fig. 6i).

3.7. *Stromatospongia norae*

Lamellate and branching processes arose from the surface of the aragonitic basal skeleton of *Stromatospongia norae* delineating so-called inter-lamellar spaces between them (Fig. 7a). The fascicular microstructure of the entire skeleton was built up by bundles of fibers, which themselves formed highly planar surfaces (Fig. 7b). However, a more granular structure became obvious at higher magnification in SEM (Fig. 7c, d, f and j). The aragonitic fibers (Fig. 7d, e) and bundles (Fig. 7f, g) of *S. norae*, showing both monocrystalline patterns (Fig. 7e', g'), were defined by abundant parallel micro-twin or stacking-fault planes domains, each aligned along

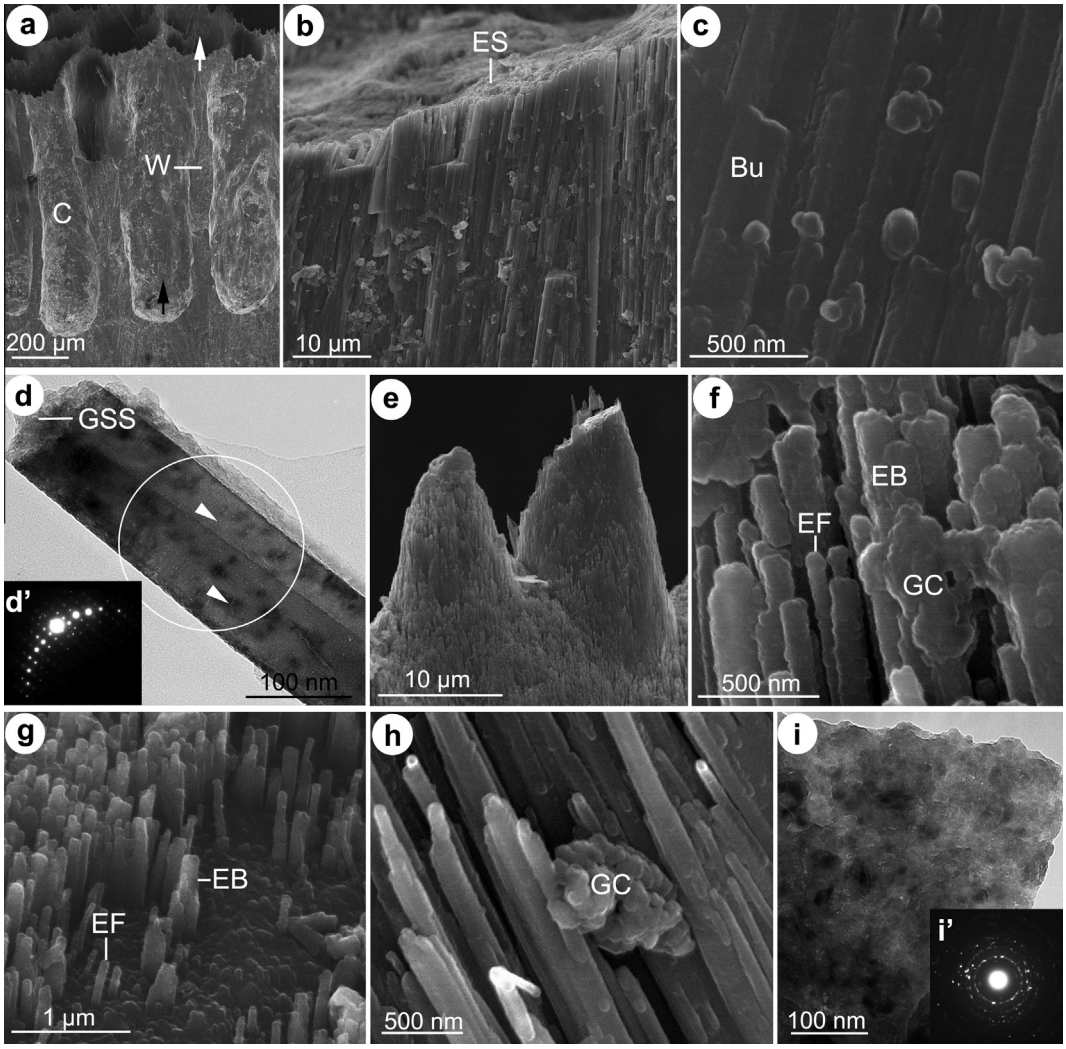

Fig.4. Aragonitic basal skeleton of *Ceratoporella nicholsoni*. (a) Macrostructure characterized by a massive basal part with apical contiguous vertical calicles. Growth zones located at the tip of walls (white arrow) and at the bottom of calicles (black arrow) (SEM). (b) Fascicular arrangement of microstructural units, bundles of fibers (SEM). (c) Higher magnifications of fibrillar bundles in the wall with granular submicronic structure (SEM). (d) Juxtaposition of two fibers composed by 20–50 nm large grains, particularly obvious in the fractured tip, and thin transverse striations (white arrowheads) (TEM). (d') SAED pattern indicating both fibers behave as a single-crystal structure (arcuate zeroth order Laue zone of reflections; white circle: SAED selection). (e) Knob-like structures at the top of the wall with growing fibers and bundles (SEM). (f) Enlargement of highly granular emerging fibers and bundles at the top of the wall with granular clusters interleaved between them (SEM). (g) Similar emerging fibers and bundles in a growing zone at the bottom of the calicle (SEM). (h) Higher magnification of emerging granular fibers and bundles at the bottom of calicle with a large interleaved cluster of grains (SEM). (i, i') Polycrystalline SAED pattern produced by randomly-arranged crystals (all concentric rings of spotty reflections; SAED selection: whole TEM picture). Bu: bundle, C: calicle, EB: emerging bundle, EF: emerging fiber, ES, external skeletal surface, GSS: granular submicronic structure, GC: granular cluster, W: wall.

their morphological axis. Such micro-twinning turned out to be coherent across very large bundles as revealed on fractured portions of the skeleton (Fig. 7f) and schematically depicted in Fig. 7h. In addition, longitudinal thin translucent material between fibers and bundles and transverse lighter striations with a step of about 5–10 nm inside both appeared during TEM observation (Fig. 7i). Finally, growing single granular fibers and bundles were emerging from the apical surface of the skeleton on superficial processes and at the bottom of inter-lamellar spaces (Fig. 7j).

3.8. *Calcifibrospongia actinostromarioides*

Branches of the reticulate basal skeleton of *Calcifibrospongia actinostromarioides* were composed of an orthogonal microstructure with bundles of fibers radiating around their longitudinal axis (Fig. 8a–c). The granular morphology in the aragonitic skeleton of this species was particularly obvious. Submicronic grains, 50–100 nm large in SEM clearly composed randomly packed clusters at the centre of the microstructure (Fig. 8c, d) as well as radiating fibers and bundles (Fig. 8c, e). While fibers and bundles have been demonstrated to be single-crystal by SAED patterns (Fig. 8f, f', g and g'), both contained thin transverse striations with lighter contrasts during their observation in TEM (Fig. 8f, g). Finally, individual emerging fibers were discrete at the growing external surface of the skeleton (Fig. 8h, i).

4. Discussion

This multi-scale mineralogical characterization of the basal skeleton of eight living hypercalcified demosponges clearly revealed several similar micronic to submicronic morphological and crystallographical features (Table 2).

Submicronic grains were the smallest structural units composing each basal skeleton investigated in this work. While SEM observations allowed distinguishing easily between 50 and 100 nm large grains and greater structural units (i.e. fibres, bundles and

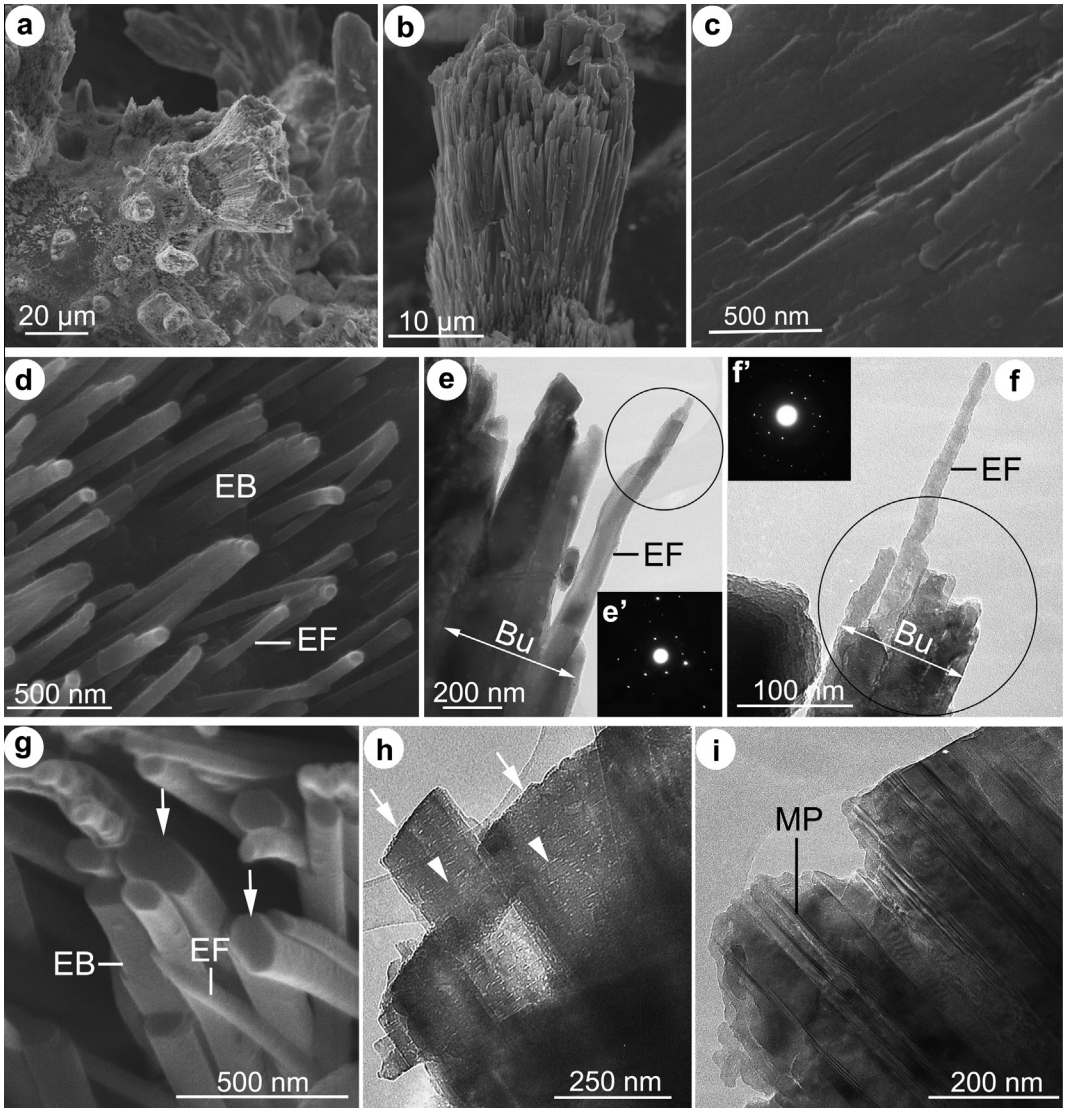

Fig.5. Aragonitic basal skeleton of *Goreauiella auriculata*. (a) Arborescent processes emerging from the reticulate macrostructural basal skeleton (SEM). (b) Detail of a process with fascicular arrangement of fibers and bundles, both characteristically slightly incurved (SEM). (c) Internal organization of fibrillar bundles presenting a granular submicronic structure (SEM). (d) External surface of the basal skeleton showing typical incurved individual emerging fibers and bundles (SEM). (e, e') Incurved emerging fiber with its previous single-crystal SAED pattern. The apparent "two-crystal" electron diffraction pattern in (e') is due to artifactual kink of the fiber under the electron beam (black circle: SAED selection) (TEM). (f, f') Coherent assemblage of fibers into larger single crystal bundle (black circle: SAED selection) (TEM). (g) Fractured bundles showing up clear planar surfaces with hexagonal outlines (white arrows) (SEM). (h) TEM evidence of thin transverse striations (white arrowheads) in large bundles with planar fractured surface (white arrows). (i) Occurrence of micro-twin planes and stacking fault planes along bundles axis cutting across granular units (TEM). Bu: bundle, EB: emerging bundle, EF: emerging fiber, MP: micro-twin plane.

clusters), their demonstration was less obvious in TEM analyses due to the superimposition of the granular structures in this crushed skeletal material. However, we still recognized granular units in TEM in very thin crushed fibers (Fig. 3h, d), at the fractured edges of fibers and bundles (Fig. 3h and (Fig. 4d) or in polycrystalline clusters (Fig. 1i, Fig. 2d, (Fig. 4i). Granular structures seemed actually smaller, ca. 20–75 nm, in TEM than in SEM. This size difference is partly explained by the ca. 15–30 nm thick carbon coating applied for appropriate SEM observation.

Submicronic grains were previously reported as the smallest structural units in the Mg-calcite basal skeleton of the Mediterranean hypercalcified sponge *P. massiliana*, belonging to the class Calcarea (Gilis et al., 2011; Stolarski and Mazur, 2005) as well as in three demosponges, *V. crypta*, *A. willeyana* and *C. nicholsoni*, using AFM (Cuif et al., 2011). Furthermore, submicronic grains have been described in several other carbonate biominerals like sponge spicules (Kopp et al., 2011; Sethmann et al., 2006), coral skeletons (e.g. Cuif and Dauphin, 2005a, 2005b; Cuif et al., 2008, 2011; Isa, 1986; Przeniosło et al., 2008; Stolarski, 2003), mollusk shells (e.g. Baronnet et al., 2008; Cuif et al., 2008, 2011; Jacob et al., 2008; Rousseau et al., 2005), brachiopod shells (e.g. Cusack et al., 2008; Goetz et al., 2011; Pérez-Huerta et al., 2013; Schmahl et al., 2012a,b) and echinoderm skeletons (Robach et al., 2005; Stolarski et al., 2009).

For each hypercalcified demosponge investigated here, submicronic grains were further organized into single-crystal fibers assembled into larger monocrystalline bundles, as in the basal skeleton of *P. massiliana* (Gilis et al., 2011). The occurrence of a crystallographic coherence along granular fibers as well as across adjacent fibers forming single-crystal bundles, observed for each basal skeleton, reinforces the crystallization propagation model previously proposed for *P. massiliana* (Gilis et al., 2011). A progressive transformation of an amorphous phase into long-range ordered single-crystals would result from the coalescence of

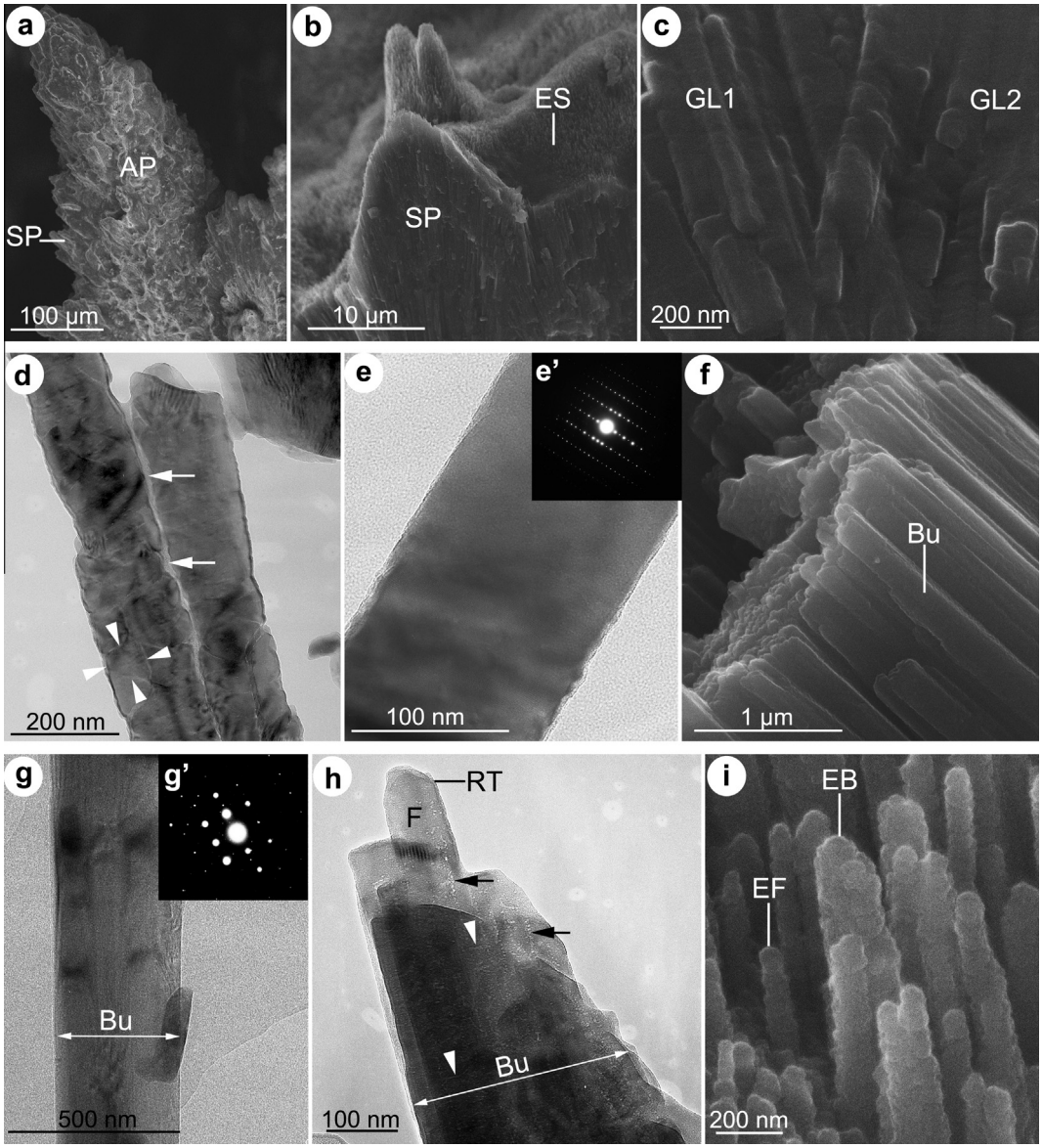

Fig.6. Aragonitic basal skeleton of *Hispidopetra miniana*. (a) Arborescent processes covering the aragonitic basal skeleton (SEM). (b) Fracture in a spike-like process showing bundles of crystalline fibers within a fascicular microstructural organization (SEM). (c) Higher magnification of radiating fibers with highly granular morphology at the interface between two differently oriented growth layers (SEM). (d) Pair of aragonitic fibers demonstrating their submicronic granular units (one is delineated by white arrowheads) and organic material at fibers boundary (white arrows) (TEM). (e, e') Detail of a single-crystal fiber (SAED selection: whole TEM picture). (f) Fracture in the fascicular microstructure showing the lateral assemblage of granular fibers into larger bundles (SEM). (g, g') Single-crystal behavior of a small fibrillar bundle (SAED selection: whole TEM picture); central interruption of Bragg contrasts crossing the bundle suggests a possible amorphous core there. (h) TEM demonstration of thin transverse striations (white arrowheads) inside bundle of fibers. Organic material located at skeletal units boundaries (black arrows). (i) Emerging highly granular fibers and bundles at the growing external surface of the basal skeleton (SEM). AP: arborescent processes, Bu: bundle, EB: emerging bundle, EF: emerging fiber, ES: external skeletal surface, F: fiber, GL: growth layer, RT: rounded tip, SP: spine-like process.

submicronic amorphous grains into organized fibers while an unknown nucleation signal would simultaneously trigger the propagation of a crystallization front from one granular unit to another within the fiber. A similar biomineralization mechanism involving crystallization propagation through submicronic amorphous granular domains was proposed to explain other single-crystal skeletal structure formation for scleractinian coral fibers (Przeniosło et al., 2008), calcitic prisms of mollusk shells (Baronnet et al. 2008; Cuif et al., 2008; Jacob et al., 2008), brachiopod shells (Cusack et al., 2008; Goetz et al., 2011; Jacob et al., 2008; Schmahl et al., 2012a,b), sea urchin larval spicules (Gong et al., 2012; Politi et al., 2008; Weiner and Addadi, 2011) and sea urchin teeth (Killian et al., 2009).

Electron-translucent materials observed in tight interstices occurring between submicronic grains of polycrystalline clusters and single-crystal fibers or bundles of all skeletons investigated became more apparent and sometimes produced small blisters when left under the electron beam, indicating a likely organic nature. This nano-scale intervened organic matrix might be a remnant of a preassembled filamentous extracellular framework orientating clusters and fibers in growing zones as previously suggested for the skeletogenesis of the Mediterranean Calcarea *P. massiliana* (Gilis et al., 2012). Other authors previously highlighted the occurrence of nano-scale organic materials at boundaries of structural units of diverse metazoan skeletons (e.g. Baronnet et al., 2008; Cuif et al., 2008, 2011; Cusack et al., 2008; Goetz

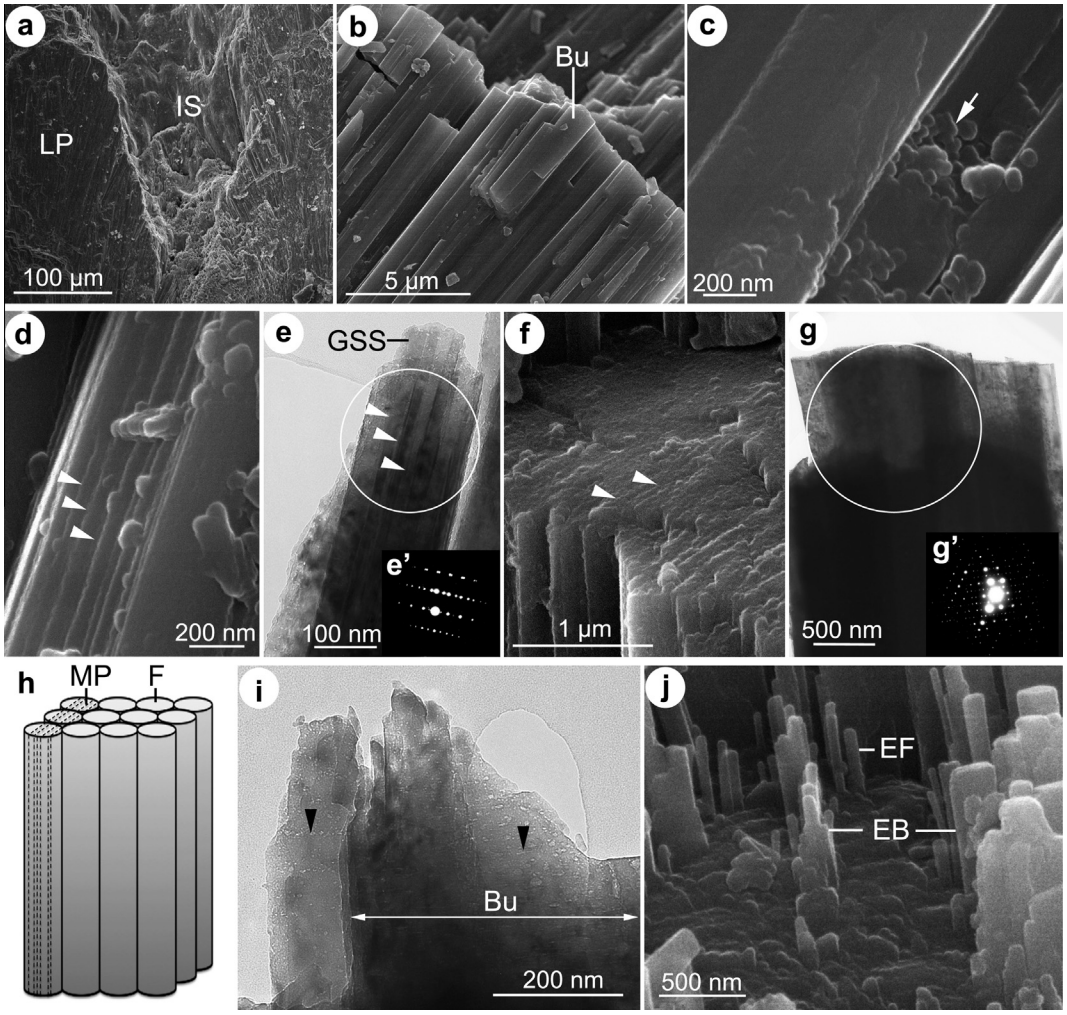

Fig.7. Aragonitic basal skeleton of *Stromatospongia norae*. (a) Macrostructure of the basal skeleton characterized by lamellate and branching processes protruding out of its surface and delimiting inter-lamellar spaces (SEM). (b) Fractured fascicular microstructure composed of bundles of fibers depicting planar surfaces at low magnification (SEM). (c) Detail of crystal bundles enhancing their submicronic granular structural units (white arrow) (SEM). (d) Micro-twin planes outcrop as parallel lines (white arrowheads) aligned along the fiber/bundle axis (SEM). (e) TEM side view of micro-twin planes (white arrowheads) oriented along the axis of the single crystal fiber that displays a multiply twinned-crystal diffraction pattern in (e') (white circle: SAED selection). Granular submicronic structures are more obvious in the fractured tip of the fiber. (f) Fractured portion of the skeleton indicating laterally coherent micro-twin planes (white arrowheads) throughout very large bundle (SEM). (g, g') Large monocrystalline fibrillar bundle composed of slightly radiating fibers (white circle: SAED selection) (TEM). (h) Schematic representation of fibrillar bundle with lateral coherence of micro-twin planes through several adjacent fibers. (i) TEM image of fibrillar bundles highlighting transverse thin striations (black arrowheads). (j) Fibers and bundles emerging from the external growing surface of the basal skeleton (SEM). Bu: bundle, EB: emerging bundle, EF: emerging fiber, F: fiber, GSS: granular submicronic structure, IS: inter-lamellar space, LP: lamellar process, MP: micro-twin plane.

et al., 2011; Griesshaber et al., 2009; Jacob et al., 2008; Nouet et al., 2012; Robach et al., 2005; Okumura et al., 2010; Rousseau et al., 2005; Schmahl et al., 2012a,b; Su et al., 2000; Suzuki et al., 2011).

Lighter transverse striations were systematically observed within fibers of each basal skeleton investigated in TEM. As these more electron-translucent striations became more pronounced under the electron beam after a few seconds to a few minutes, they might similarly be related to very sensitive material like thin organic fibrils located within the single-crystal units. Depending on the species, bands were distant by 2–15 nm. Furthermore, striations were not perfectly continuous linear structures across the fibers, but intermittent ones, with a more or less sinuous pattern revealed at higher magnification. As these thin striations were transversal to the fiber axis and particularly to series of constituting submicronic grains, they could not be related to the above-described organic material enveloping structural units. To our knowledge, this is the first description of transverse nanoscale lighter striations within a single crystal calcium carbonate biomineral, although very similar contrasts are visible in the calcitic primary shell layer of the brachiopod *Gryphus vitreus* (“white spots”; Fig. 3b in Goetz et al., 2011). In *A. wellsi*, transverse striations were revealed only under dark field imaging conditions, a method highly sensitive to detect faint local distortions of the crystal lattice. This could as well result from the occurrence of transverse organic material in these calcitic skeletons. Such local strains could be related to the strong binding interaction between the organic and crystalline components of the organo-mineral composite.

A single set of {1 1 0} micro-twin or stacking fault planes was observed in most aragonitic skeletons investigated herein, but not in calcitic ones. These micro-twin planes were always aligned along the longitudinal axis of fibers, and were therefore continuous throughout constituting submicronic granular units when the latter were crystallographically aligned.

Micro-twin planes were recently described in biogenic aragonite (Suzuki et al., 2012) and more particularly in various bivalves and gastropods shells presenting crossed-lamellar aragonitic layers (Kobayashi and Akai, 1994; Mukai et al., 2010; Nouet et al., 2012;

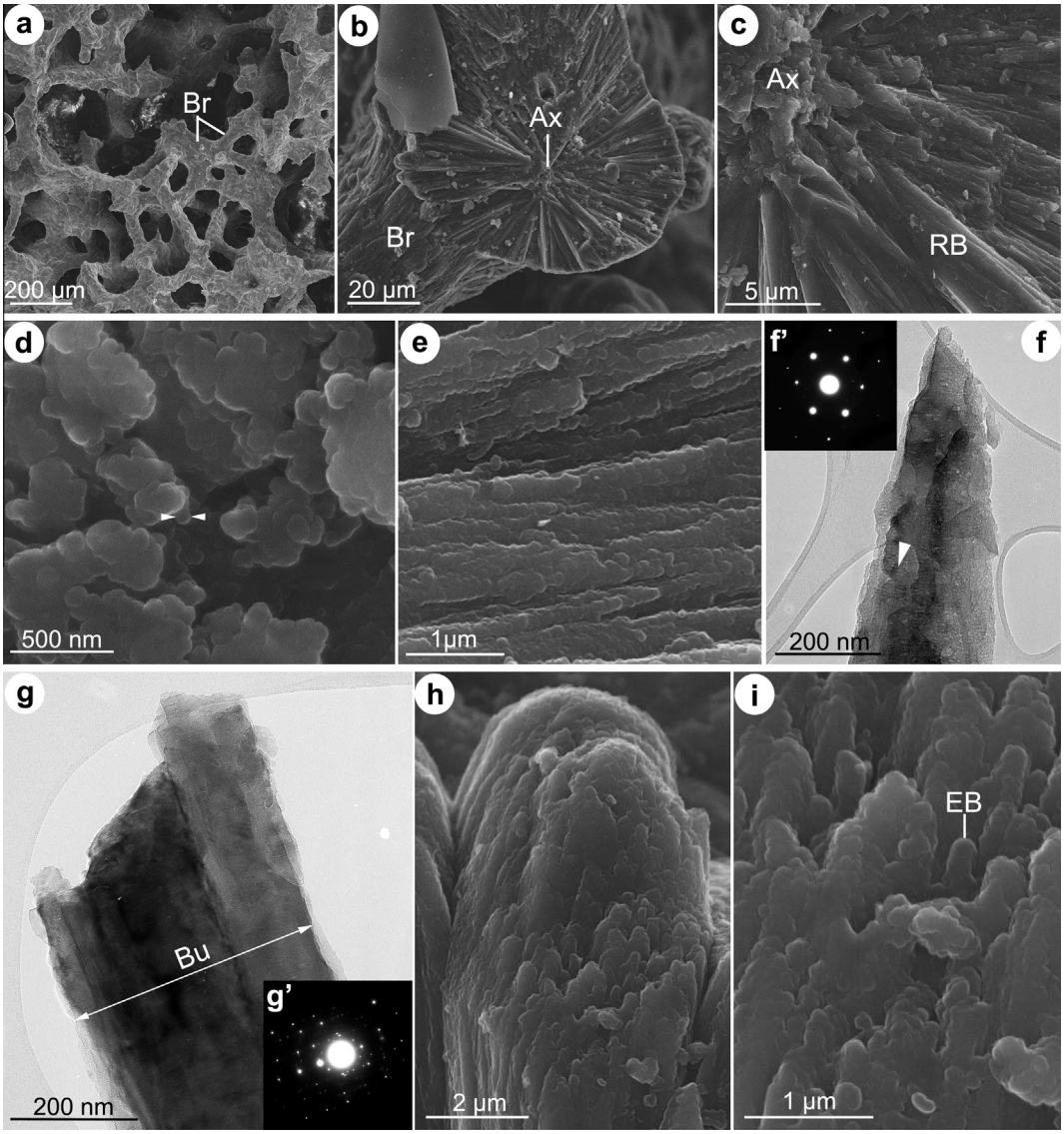

Fig.8. Aragonitic basal skeleton of *Calcifibrospongia actinostromarioides*. (a) Reticulate macrostructural organization of the basal skeleton (SEM). (b) Branch of the reticulate skeleton in transverse fracture indicating an orthogonal microstructure with bundles of fibers radiating out around the longitudinal axis of the branch (SEM). (c) Enlargement of (b) illustrating the granular submicronic structure of the branch axis and of radiating fibers (SEM). (d) Detail of clusters of submicronic grains (white arrowheads) composing the axis of the orthogonal microstructure (SEM). (e) Highly granular morphology of radiating fibrillar bundles (SEM). (f) Superposition of fibers with transverse thin striations (white arrowheads) extending across granular submicronic units (TEM). (f') SAED pattern indicating single-crystal behavior of superposed fibers (SAED selection: whole TEM picture). (g, g') Bundles of fibers with mostly monocrystalline patterns (SAED selection: whole TEM picture). (h) External growing surface of the reticulate skeleton (SEM). (i) Enlargement of the external surface showing less obvious emerging fibers and bundle due to the highly granular morphology (SEM). Ax: axis, Br: branch, Bu: bundle, EB: emerging bundle, RB: radiating bundles.

Suzuki et al., 2010; Wilmot et al., 1992). Nouet et al. (2012) demonstrated that micro-twin planes could not result from mechanical stress on crystals but would correspond to growth twinning formed during crystallization. In addition, as these authors also noticed the perfect continuity of twin planes through granular submicronic units in the aragonitic structures of the shell, they conclude that crystallization propagation through granular units would occur after the assemblage of the latter. Similarly, we suggest that crystallization propagation in hypercalcified demosponges might also occur after the assemblage of amorphous grains into higher structural units.

Emerging individual granular fibers were observed on growing superficial surfaces of every aragonitic basal skeleton investigated here. On one hand, this unusual feature reinforces the presumption that skeletal fibers are real structural units of an early growth stage of the basal skeleton formation. On the other hand, that the latter might not be considered as a strictly stationary growth, that would have led to a perfectly plane growing surface. However, it is uncertain whether this most superficial skeletal layer truly relates to a native growing organization state or if it results from a preferential dissolution, during soft tissue removal by sodium hypochlorite, of a more soluble organic and/or inorganic material previously existing between these crystalline emerging skeletal elements. The use of cryo-methods for the preparation of organic and skeletal material in biomineralizing systems might significantly improve the preservation of the native structural organization of such growing skeletal layers to elucidate their formation pathways (Addadi et al., 2012; Mahamid et al., 2010, 2011; Nudelman et al., 2008; Sone et al. 2007).

In addition to the mineralogical characters shared by the eight demosponges examined in this work, both *Acanthochaetetes wellsi* and *Astrosclera willeyana* presented particular features.

A. wellsi typically displayed a more electron-translucent longitudinal core in Mg-calcite fibers found in all parts of its basal skeleton. Previous investigations of this species concluded that knobby crystalline fibers, found on walls only, are built up from of a row of seed crystals up to 60 nm long, likely relating to the herein described submicronic grains. These would form on a collagenous "cooked spaghetti" shaped template (*sensu* Reitner and Gautret, 1996); the latter eventually remaining in the skeletal structure (Gautret et al., 1996; Reitner et al., 2001; Wörheide et al., 1996). Nevertheless, this incorporated organic template could not correspond to the translucent axial core observed here, as the latter appeared crystalline in TEM. The likely occurrence of a thin organic material around this longitudinal core and its nature still needs to be elucidated. Finally, the highly similar morphological features and organization of fibers observed here in walls and tabulae in *A. wellsi*, suggest that they are produced by a shared biomineralization mechanism.

A. willeyana is the only known species to date involving an intracellular pathway to produce its spherulitic basal skeleton, which is followed by an extracellular growth (Lister, 1900; Wörheide, 1998; Wörheide et al., 1997). While different biomineralization mechanisms were proposed to explain these growth phases (Jackson et al., 2010; Wörheide, 1998), in the present mineralogical characterization of the basal skeleton of *A. willeyana*, both the intracellularly and all extracellularly produced aragonitic fibers of spherulites were identically composed of submicronic 30–100 nm granular structural units. Furthermore, no clear distinction in the structural organization of any of these granular fibers was noticed. Accordingly, even if their formation involved two different cell types (large vesicle cells and basopinacocytes; Wörheide, 1998), a similar biological control leading to the formation of identical submicronic granular structures might be involved.

Beside shared mineralogical features at the submicron- and nano-scales, every basal skeleton investigated here showed very specific micro- and macrostructural organizations. For example, the morphology of fibers was specific to each demosponge species with sizes varying between 50 to 200 nm in diameter and from a few hundred nanometers to a few hundred micrometers in length. For some species, they were highly granular and therefore less easily recognized (*W. caicosensis, H. miniana and C. actinostromarioides*), for others they were more linear and regular (*A. willeyana, C. nicholsoni and S. norae*), or slightly curved (*G. auriculata*) or even presented a specific longitudinal core (*A. wellsi*). As every basal skeleton investigated here were likely to be built up under a strict biological control, there is good evidence to believe that the observed variations might result from different cellular controls and organic matrix compositions arising themselves from the genetical diversity of the eight species. While biological investigations of living hypercalcified sponges are quite scarce, it is obvious that different cell types (e.g. basopinacocytes, vacuolar cells and granular cells) could be involved in the biomineralization of basal skeletons (Gilis et al., 2011; Reitner and Gautret, 1996; Willenz and Hartman, 1989; Willenz and Pomponi, 1996; Wörheide, 1998); in *A. willeyana* and *A. wellsi*, even two additional cell types were reported (Reitner and Gautret, 1996; Wörheide, 1998). Furthermore, according to the species, even a same cell type, e.g. basopinacocytes, might control differently basal skeleton formation by producing organic matrices with various organizations and chemical compositions, as reported for several hypercalcified demosponges (Bergbauer et al., 1996; Cuif and Gautret, 1991; Gautret et al., 1996; Lange et al., 2001; Reitner et al., 2001).

Finally, for three Recent demosponge species investigated herein, *A. willeyana*, *C. nicholsoni* and *A. wellsi,* fossil relatives have been found in Triassic and Cretaceous records (Cuif et al., 1979; Cuif and Gautret, 1991; Cuif et al., 2011; Hartman, 1979; Reitner, 1992; Wood and Reitner, 1986; Wörheide, 1998). Pointing out strong similarities in the chemistry, microstructure and mode of formation of the basal skeleton between living and fossil specimens, these authors suggested that biomineralization might be an ultra-conservative process preserved for million of years in these species and assigned them to "living fossils". Biomineralization pathways at the origin of the shared mineralogical features highlighted in the present work might already be running in the fossil counterparts of these three living species. By extension, we suggest that all hypercalcified species belonging to both Demospongiae and Calcarea might have inherited the basic features of their biologically controlled biomineralization from early Palaeozoic ancestors. This statement is reinforced by the recent AFM demonstration of submicronic grains as the smallest structural units in a well preserved Stromatoporoid fossil from the Devonian period (Cuif et al., 2011). A more extensive examination of basal skeletons at the submicronic scale of very diverse fossil records could further support the hypothetical occurrence of a universal and preserved toolkit of biomineralization among almost all hypercalcified sponges.

As a conclusion, this comparative mineralogical study of eight hypercalcified demosponges belonging to phylogenetically distant taxa among Porifera, the Phylum considered as the most ancient of metazoans (Wang et al., 2010), supports the well reported theory of an ubiquitous biomineralization mechanism among invertebrates, leading to species-specific microstructural units with long-range crystallographic coherence (e.g. Cuif et al., 2011; Weiner and Addadi, 2011; Schmahl et al., 2012b). This process involves simultaneously submicronic grains of calcium carbonate as the smallest structural units, nano-scale organic matrices to control their specific assemblage and crystallization propagation through these organized submicronic granular units.

Acknowledgments

We thank Claude Henry for accessing the microscopy facilities of the Centre Interdisciplinaire de Nanosciences de Marseille (CINaM). This work was chronologically supported by NSF Grant BSR-8317690 to Yale University, a NATO Science fellowship, a subvention of the Foundation Agathon de Potter, a Lerner Gray Grant for Marine Research, and a travel grant from the Fonds Léopold III pour l'Exploration et la Conservation de la Nature to Ph. Willenz, the CALMARS II project (No. SD/CS/02A-) from the Belgian Federal Science Policy and by FRFC contract (No. 2-4532.07-). We thank all members of the Discovery Bay Marine Laboratory for optimal diving and laboratory conditions during our stays in Jamaica. We are indebted to R. Colwell and D. Santavy, Department of Microbiology, University of Maryland for their invitation to join a cruise on the ORV Cape Florida to Acklins Island, where the specimen of *C. actinostromarioides* was found. S. Pomponi, Harbor Branch Oceanographic Institution, is thanked for giving Ph. Willenz the possibility to join a cruise to Turks and Caicos Islands where *W. caicosensis* was discovered thanks to the patient assistance of the crew of the RIV Edwin Link and Johnson-Sea Link I during samples collection. M. Kelly and C. Valentine, British Museum of Natural History, generously donated us the samples of *A. wellsi* and *A. willeyana* used in this work. Ph. Dubois is a Senior Research Associate of the Fund for Scientific Research of Belgium (F.R.S.-*FNRS*). M. Gilis benefits a FRIA PhD grant conceded by the FNRS (Belgium).

References

Addadi, L., Vidavsky, N., Weiner, S., 2012. Transient precursor amorphous phases in biomineralization. In the footsteps of Heinz A. Lowenstam. Z. Kristallogr. 227, 711–717.

Baronnet, A., Cuif, J.-P., Dauphin, Y., Farre, B., Nouet, J., 2008. Crystallization of biogenic Ca-carbonate within organo-mineral micro-domains. Structure of the calcite prisms of the Pelecypod *Pinctada margaritifera* (Mollusca) at the submicron to nanometre ranges. Mineral. Mag. 72, 539–548.

Beniash, E., Aizenberg, J., Addadi, L., Weiner, S., 1997. Amorphous calcium carbonate transforms into calcite during sea urchin larval spicule growth. Proc. R. Soc. Lond. Ser. B: Biol. Sci. 264, 461–465.
Bergbauer, M., Lange, R., Reitner, J., 1996. Characterization of oganic matrix proteins enclosed in high Mg-calcite crystals of the coralline sponge Spirastrella (Acanthochaetetes) wellsi. In: Reitner, J., Neuweiler, F., Gunkel, F. (Eds.), Global and Regional Controls on Biogenic Sedimentation. I. Reef Evolution, Research Reports, Goett. Arb. Geol. Palaeontol. 2, pp. 9–12.
Cuif, J.-P., Dauphin, Y., 2005a. The environment recording unit in coral skeletons – a synthesis of structural and chemical evidences for a biochemically driven, stepping-growth process in fibres. Biogeosciences 2, 61–73.
Cuif, J.-P., Dauphin, Y., 2005b. The two-step mode of growth in the scleractinian coral skeletons from the micrometre to the overall scale. J. Struct. Biol. 150, 319–331.
Cuif, J.-P., Gautret, P., 1991. Taxonomic value of microstructural features in calcified tissue from Recent and fossil Demospongiae and Calcarea. In: Reitner, J., Keupp, H. (Eds.), Fossil and Recent Sponges. Springer-Verlag, Berlin, pp. 159–169.
Cuif, J.-P., Debrenne, F., Lafuste, J.G., Vacelet, J., 1979. Comparaison de la microstructure du squelette carbonaté non spiculaire d'éponges actuelles et fossiles. In: Lévi, C., Boury-Esnault, N. (Eds.), Biologie des Spongiaires – Sponge Biology. Colloques Internationaux du Centre National de la Recherche Scientifique, CNRS, Paris, pp. 459–465.
Cuif, J.P., Dauphin, Y., Farre, B., Nehrke, G., Nouet, J., et al., 2008. Distribution of sulphated polysaccharides within calcareous biominerals suggests a widely shared two-step crystallization process for the microstructural growth units. Mineral. Mag. 72, 233–237.
Cuif, J.-P., Dauphin, Y., Sorauf, J.E., 2011. Biominerals and Fossils through Time. Cambridge University Press, Cambridge.
Cusack, M., Dauphin, Y., Chung, P., Perez-Huerta, A., Cuif, J.P., 2008. Multiscale structure of calcite fibres of the shell of the brachiopod *Terebratulina retusa*. J. Struct. Biol. 164, 96–100.
Gautret, P., Reitner, J., Marin, F., 1996. Mineralization events during growth of the coralline sponges Acanthochaetetes and Vaceletia. Bull. Inst. Océanogr. 14, 325–334, Monaco. N° Spécial.
Gilis, M., Grauby, O., Willenz, Ph., Dubois, Ph., Legras, L., et al., 2011. Multi-scale mineralogical characterization of the hypercalcified sponge *Petrobiona massiliana* (Calcarea, Calcaronea). J. Struct. Biol. 176, 315–329.
Gilis, M., Baronnet, A., Dubois, Ph., Legras, L., Grauby, O., et al., 2012. Biologically controlled mineralization in the hypercalcified sponge *Petrobiona massiliana* (Calcarea, Calcaronea). J. Struct. Biol. 178, 279–289.
Goetz, A.J., Steinmetz, D.R., Griesshaber, E., Zaefferer, S., Raabe, D., et al., 2011. Interdigitating biocalcite dendrites form a 3-D jigsaw structure in brachiopod shells. Acta Biomater. 7, 2237–2243.
Gong, Y.U.T., Killian, C.E., Olson, I.C., Appathurai, N.P., Amasino, A.L., et al., 2012. Phase transitions in biogenic amorphous calcium carbonate. Proc. Natl. Acad. Sci. USA 109, 6088–6093.
Griesshaber, E., Kelm, K., Sehrbrock, A., Mader, W., Mutterlose, J., et al., 2009. Amorphous calcium carbonate in the shell material of the brachiopod Megerlia truncata. Eur. J. Mineral. 21, 715–723.
Hartman, W.D., 1969. New genera and species of coralline sponges (Porifera) from Jamaica. Postilla 137, 1–39.
Hartman, W.D., 1979. A new sclerosponge from the Bahamas and its relationship to Mesozoic stromatoporoids. In: Lévi, C., Boury-Esnault, N. (Eds.), Biologie des Spongiaires – Sponge Biology. Colloques Internationaux du Centre National de la Recherche Scientifique, CNRS, Paris, pp. 467–474.
Hartman, W.D., Goreau, T.F., 1970. Jamaican coralline sponges: their morphology, ecology and fossil relatives. Symp. Zool. Soc. Lond. 25, 205–243.
Hartman, W.D., Goreau, T.F., 1975. A Pacific tabulate sponge, living representative of a new order of sclerosponges. Postilla 167, 1–21.
Hartman, W.D., Goreau, T.F., 1976. A new ceratoporellid sponge (Porifera: Sclerospongiae) from the Pacific. In: Harrison, F.W., Cowden, R.R. (Eds.), Aspects of Sponge Biology. Academic Press, New York & London, pp. 329–347.
Isa, Y., 1986. An electron microscope study on the mineralization of the skeleton of the staghorn coral *Acropora hebes*. Mar. Biol. 93, 91–101.
Jackson, D.J., Thiel, V., Wörheide, G., 2010. An evolutionary fast-track to biocalcification. Geobiology 8, 191–196.
Jackson, D.J., Macis, L., Reitner, J., Worheide, G., 2011. A horizontal gene transfer supported the evolution of an early metazoan biomineralization strategy. BMC Evol. Biol. 11, 238.
Jacob, D.E., Soldati, A.L., Wirth, R., Huth, J., Wehrmeister, U., et al., 2008. Nanostructure, composition and mechanisms of bivalve shell growth. Geochim. Cosmochim. Acta 72, 5401–5415.
Killian, C.E., Metzler, R.A., Gong, Y.U.T., Olson, I.C., Aizenberg, J., et al., 2009. Mechanism of calcite co-orientation in the sea urchin tooth. J. Am. Chem. Soc. 131, 18404–18409.
Kobayashi, I., Akai, J., 1994. Twinned aragonite crystals found in the bivalvian crossed lamellar shell structure. J. Geol. Soc. Jpn. 100, 177–180.
Kopp, C., Meibom, A., Beyssac, O., Stolarski, J., Djediat, S., et al., 2011. Calcareous sponge biomineralization: ultrastructural and compositional heterogeneity of spicules in *Leuconia johnstoni*. J. Struct. Biol. 173, 99–109.
Lange, R., Bergbauer, M., Szewzyk, U., Reitner, J., 2001. Soluble proteins control growth of skeleton crystals in three coralline demosponges. Facies 45, 195–202.
Lister, J.J., 1900. *Astrosclera willeyana*, the type of a new family of sponges. In: Willey, A. (Ed.), Zoological Results Based on Material from New Britain New Cuinea, Loyalty Islands and Elsewhere. Collected During the Years 1895, 1896 and 1897, vol. 4. Cambridge University Press, Cambridge, pp. 459–482, pls XLV–XLVIII.
Ma, Y.R., Weiner, S., Addadi, L., 2007. Mineral deposition and crystal growth in the continuously forming teeth of sea urchins. Adv. Funct. Mater. 17, 2693–2700.
Mahamid, J., Aichmayer, B., Shimoni, E., Ziblat, R., Li, C., et al., 2010. Mapping amorphous calcium phosphate transformation into crystalline mineral from the cell to the bone in zebrafish fin rays. Proc. Natl. Acad. Sci. USA 107, 6316–6321.
Mahamid, J., Sharir, A., Gur, D., Zelzer, E., Addadi, L., et al., 2011. Bone mineralization proceeds through intracellular calcium phosphate loaded vesicles: a cryo-electron microscopy study. J. Struct. Biol. 174, 527–535.
Mukai, H., Saruwatari, K., Nagasawa, H., Kogure, T., 2010. Aragonite twinning in gastropod nacre. J. Cryst. Growth 312, 3014–3019.
Nouet, J., Baronnet, A., Howard, L., 2012. Crystallization in organo-mineral micro-domains in the crossed-lamellar layer of *Nerita undata* (Gastropoda, Neritopsina). Micron 43, 456–462.
Nudelman, F., Shimoni, E., Klein, E., Rousseau, M., Bourrat, X., et al., 2008. Forming nacreous layer of the shells of the bivalves *Atrina rigida* and *Pinctada margaritifera*: an environmental- and cryo-scanning electron microscopy study. J. Struct. Biol. 162, 290–300.
Okumura, T., Suzuki, M., Nagasawa, H., Kogure, T., 2010. Characteristics of biogenic calcite in the prismatic layer of a pearl oyster, *Pinctada fucata*. Micron 41, 821–826.
Pérez-Huerta, A., Dauphin, Y., Cusack, M., 2013. Biogenic calcite granules–are brachiopods different? Micron 44, 395–403.
Politi, Y., Arad, T., Klein, E., Weiner, S., Addadi, L., 2004. Sea urchin spine calcite forms via a transient amorphous calcium carbonate phase. Science 306, 1161–1164.
Politi, Y., Levi-Kalisman, Y., Raz, S., Wilt, F., Addadi, L., et al., 2006. Structural characterization of the transient amorphous calcium carbonate precursor phase in sea urchin embryos. Adv. Funct. Mater. 16, 1289–1298.
Politi, Y., Metzler, R.A., Abrecht, M., Gilbert, B., Wilt, F.H., et al., 2008. Transformation mechanism of amorphous calcium carbonate into calcite in the sea urchin larval spicule. Proc. Natl. Acad. Sci. USA 105, 17362–17366.
Przeniosło, R., Stolarski, J., Mazur, M., Brunelli, M., 2008. Hierarchically structured scleractinian coral biocrystals. J. Struct. Biol. 161, 74–82.
Raz, S., Hamilton, P.C., Wilt, F.H., Weiner, S., Addadi, L., 2003. The transient phase of amorphous calcium carbonate in sea urchin larval spicules: the involvement of proteins and magnesium ions in Its formation and stabilization. Adv. Funct. Mater. 13, 480–486.
Reitner, J., 1992. "Coralline Spongien" Der Versuch einer phylogenetisch–taxonomischen analyse. Coralline sponges an attempt of a phylogenetic–taxonomic analysis. Berl. Geowiss. Abh. Reihe E Palaeobiol. 1, 1–352.
Reitner, J., Engeser, T., 1987. Skeletal structures and habitats of recent and fossil *Acanthochaetetes* (sub-class Tetractinomorpha, Demospongiae, Porifera). Coral Reefs 6, 13–18.
Reitner, J., Gautret, P., 1996. Skeletal formation in the modern but ultraconservative chaetetid sponge *Spirastrella* (*Acanthochaetetes*) *wellsi* (Demospongiae, Porifera). Facies 34, 193–208.
Reitner, J., Wörheide, G., Lange, R., Thiel, V., 1997. Biomineralization of calcified skeletons in three Pacific coralline demosponges- an approach to the evolution of basal skeletons. Cour. Forsch. Inst. Senckenberg 201, 371–383.
Reitner, J., Wörheide, G., Lange, R., Kindel, G.S., 2001. Coralline demosponges – a geobiological portrait. Bull. Tohoku Univ. Mus. 1 (219), 235.
Robach, J.S., Stock, S.R., Veis, A., 2005. Transmission electron microscopy characterization of macromolecular domain cavities and microstructure of single-crystal calcite tooth plates of the sea urchin *Lytechinus variegatus*. J. Struct. Biol. 151, 18–29.
Rousseau, M., Lopez, E., Stempflé, P., Brendlé, M., Franke, L., et al., 2005. Multiscale structure of sheet nacre. Biomaterials 26, 6254–6262.
Schmahl, W.W., Griesshaber, E., Kelm, K., Goetz, A., Jordan, G., et al., 2012a. Hierarchical structure of marine shell biomaterials: biomechanical functionalization of calcite by brachiopods. Z. Kristallogr. – Cryst. Mater. 227, 793–804.
Schmahl, W.W., Griesshaber, E., Kelm, K., Ball, A., Goetz, A., et al., 2012b. Towards systematics of calcite biocrystals: insight from the inside. Zeitschrift für Kristallographie - Crystalline Materials. 227, 604–611.
Sethmann, I., Wörheide, G., 2008. Structure and composition of calcareous sponge spicules: a review and comparison to structurally related biominerals. Micron 39, 209–228.
Sethmann, I., Hinrichs, R., Wörheide, G., Putnis, A., 2006. Nano-cluster composite structure of calcitic sponge spicules—a case study of basic characteristics of biominerals. J. Inorg. Biochem. 100, 88–96.
Sone, E.D., Weiner, S., Addadi, L., 2007. Biomineralization of limpet teeth: a cryo-TEM study of the organic matrix and the onset of mineral deposition. J. Struct. Biol. 158, 428–444.
Stolarski, J., 2003. Three-dimensional micro- and nanostructural characteristics of the scleractinian coral skeleton: a biocalcification proxy. Acta Palaeontol. Pol. 48, 497–530.
Stolarski, J., Mazur, M., 2005. Nanostructure of biogenic *vs* abiogenic calcium carbonate crystals. Acta Palaeontol. Pol. 50, 847–865.
Stolarski, J., Gorzelak, P., Mazur, M., Marrocchi, Y., Meibom, A., 2009. Nanostructural and geochemical features of the Jurassic isocrinid columnal ossicles. Acta Palaeontol. Pol. 54, 69–75.
Su, X., Kamat, S., Heuer, A.H., 2000. The structure of sea urchin spines, large biogenic single crystals of calcite. J. Mater. Sci. 35, 5545–5551.

Suzuki, M., Kameda, J., Sasaki, T., Saruwatari, K., Nagasawa, H., et al., 2010. Characterization of the multilayered shell of a limpet, *Lottia kogamogai* (Mollusca: Patellogastropoda), using SEM–EBSD and FIB–TEM techniques. J. Struct. Biol. 171, 223–230.

Suzuki, M., Okumura, T., Nagasawa, H., Kogure, T., 2011. Localization of intracrystalline organic macromolecules in mollusk shells. J. Cryst. Growth 337, 24–29.

Suzuki, M., Kim, H., Mukai, H., Nagasawa, H., Kogure, T., 2012. Quantitative XRD analysis of 110 twin density in biotic aragonites. J. Struct. Biol. 180, 458–468.

Vacelet, J., 1964. Étude monographique de l'Éponge Calcaire Pharétronide de Méditerranée, Petrobiona massiliana Vacelet et Lévi. Les Pharétronides actuelles et fossiles. Rec. Trav. Stat. Mar. Endoume 34, 1–125.

Vacelet, J., 1970. Les éponges pharétronides actuelles. In: Fry, W.G. (Ed.), The Biology of the Porifera. Symposia of the Zoological Society of London, Academic Press, London, pp. 189–204.

Vacelet, J., 1979. Description et affinités d'une éponge actuelle. In: Lévi, C., Boury-Esnault, N. (Eds.), Biologie des Spongiaires - Sponge Biology. Colloques Internationaux du Centre National de la Recherche Scientifique, CNRS, Paris, pp. 483–493.

Vacelet, J., 1983. Les Éponges calcifiées et les récifs anciens. Pour la Sci. 68, 14–22.

Vacelet, J., 1985. Coralline sponges and the evolution of Porifera. In: Conway Morris, S. et al. (Eds.), The Origins and Relationships of Lower Invertebrates. Clarendon Press, Oxford, pp. 1–13.

Vacelet, J., Lévi, C., 1958. Un cas de survivance, en Méditerranée, du groupe d'éponges fossiles des pharétronides. C. R. hebd. Séanc. Acad. Sci. Paris Ser. II 246, 318–320.

Vacelet, J., Willenz, Ph., Hartman, W.D., 2010. Living hypercalcified sponges. Treatise of Paleontology, The University of Kansas Paleontological Institute, Treatise Online, Part E, Revised, vol. 4, pp. 1–16.

van Soest, R.W.M., Boury-Esnault, N., Vacelet, J., Dohrmann, M., Erpenbeck, D., et al., 2012. Global diversity of sponges (Porifera). PLoS One 7, 1–23.

Wang, X., Hu, S., Gan, L., Wiens, M., Müller, W.E.G., 2010. Sponges (Porifera) as living metazoan witnesses from the Neoproterozoic: biomineralization and the concept of their evolutionary success. Terra Nova. 22, 1–11.

Wehrmeister, U., Jacob, D.E., Soldati, A.L., Loges, N., Häger, T., et al., 2011. Amorphous, nanocrystalline and crystalline calcium carbonates in biological materials. J. Raman Spectrosc. 42, 926–935.

Weiner, S., Addadi, L., 2011. Crystallization pathways in biomineralization. Annu. Rev. Mater. Res. 41, 21–40.

Weiss, I.M., Tuross, N., Addadi, L., Weiner, S., 2002. Mollusc larval shell formation: Amorphous calcium carbonate is a precursor phase for aragonite. J. Exp. Zool. 293, 478–491.

Willenz, Ph., Hartman, W.D., 1989. Micromorphology and ultrastructure of caribbean sclerosponges. I. *Ceratoporella nicholsoni* and *Stromatospongia norae* (Ceratoporellidae: Porifera). Mar. Biol. 103, 387–401.

Willenz, Ph., Pomponi, S.A., 1996. A new deep sea coralline sponge from Turks & Caicos Islands: Willardia caicosensis gen. et sp. nov. (Demospongiae: Hadromerida). In: Ph. Willenz (Ed.), Recent Advances in Sponge Biodiversity Inventory and Documentation, Bull. Inst. R. Sci. Nat. Belg. Biol. vol. 66 (Suppl.), pp. 205–218.

Wilmot, N.V., Barber, D.J., Taylor, J.D., Graham, A.L., 1992. Electron microscopy of molluscan crossed-lamellar microstructure. Philos. Trans. R. Soc. Lond. B Biol. Sci. 337, 21–35.

Wood, R.A., Reitner, J., 1986. Poriferan affinities of Mesozoic stromatoporoids. Palaeontol 29, 469–473.

Wörheide, G., 1998. The reef cave dwelling ultraconservative coralline demosponge *Astrosclera willeyana* LISTER 1900 from the Indo-Pacific. Micromorphology, ultrastructure, biocalcification, isotope record, taxonomy, biogeography, phylogeny. Facies 38, 1–88.

Wörheide, G., Reitner, J., Gautret, P., 1996. Biocalcification processes in three coralline sponges from the Lizard Island section (Great Barrier Reef, Australia): the Stromatoporoid Astrosclera, the Chaetetid Spirastrella (Acanthochaetetes) and the Sphinctozoid Vaceletia (Demospongiae). In: Reitner, J., Neuweiler, F., Gunkel, F. (Eds.), Global and Regional Controls on Biogenic Sedimentation. 1. Reef Evolution, Research Reports, Goett. Arb. Geol. Palaeontol., vol. 2, pp. 149–153.

Wörheide, G., Reitner, J., Gautret, P., 1997. Comparison of biocalcification processes in the two coralline demosponges Astrosclera willeyana Lister 1900 and "Acanthochaetetes" wellsi Hartman and Goreau 1975. In: Lessios, H.A., Macintyre, I.G. (Eds.), Proceedings of Eighth International Coral Reef Congress, Smithsonian Tropical Research Institute, Panama, pp. 1427–1432.